Macromolecules ARTICLE

Macromolecules **2010**, *43*, 6067–6074 **6067**
DOI: 10.1021/ma1007573

Morphology of Injection-Molded Isotactic Polypropylene/Silica Composites Prepared via *in-Situ* Sol−Gel Technology

Xiaomin Zhu,*,† Claudiu Melian,† Qizheng Dou,† Karin Peter,† Dan E. Demco,† Martin Möller,† Denis V. Anokhin,‡ Jean-Marc Le Meins,‡ and Dimitri A. Ivanov*,‡

†DWI an der RWTH Aachen e.V. und Institut für Technische und Makromolekulare Chemie der RWTH Aachen, Pauwelsstr. 8, D-52056 Aachen, Germany, and ‡Institut de Sciences des Matériaux de Mulhouse, IS2M CNRS LRC 7228, 15 rue Jean Starcky, F-68057 Mulhouse, France

Received April 8, 2010; Revised Manuscript Received June 4, 2010

ABSTRACT: We report on the semicrystalline morphology of injection-molded isotactic polypropylene (iPP)/silica composites prepared via *in situ* sol−gel technology using hyperbranched polyethoxysiloxane as a silica precursor. The microstructural analysis has been carried out with a combination of small- and wide-angle X-ray scattering and ^{1}H solid-state NMR spectroscopy. The *in situ* formed silica particles significantly alter the semicrystalline morphology of iPP by improving orientation of the "mother" crystals in the sample core simultaneously with an increase of the "daughter" crystal fraction. Moreover the particles induce formation of thicker crystalline domains and growth of β-crystals in the sample core. The observed morphological modifications can be accounted for by a 2-fold effect of the silica particles, i.e., their action as a nucleating agent of the β-phase, on the one hand, and as a lubrificant reducing the polymer melt viscosity, on the other. Proton spin-diffusion experiment using a double-quantum filter was found suitable for the measurement of the chain mobility gradient in the interface region. The results obtained indicate enhanced polymer chain mobility in the amorphous region in the presence of the silica particles. Finally, the morphology and chain dynamics of the iPP/silica composites are correlated to mechanical properties of the injection-molded samples.

1. Introduction

Incorporation of inorganic micro- and nanoparticles into polymer matrices is a well-established approach for improvement of material properties[1−3] such as reinforcement of thermoplastic and thermosetting polymers, enhancement of thermal stability and fire resistance, and increase of barrier properties. As described by Einstein's theory, the viscosity of a composite increases with volume fraction of the filler.[4] However, it has been recently demonstrated that ultrasmall nanoparticles homogeneously distributed in the polymer matrix can effectively reduce the polymer melt viscosity.[5−7] The viscosity decrease was attributed in this case to increased free volume induced by the nanoparticles addition. By measuring the diffusion coefficient of nanoparticles in the polymer melt using dynamic X-ray scattering, it has been concluded that the nanoparticles diffuse faster than the entangled mesh and so do not participate in its dynamics; they merely occupy space to provide a constraint release mechanism via dilution.[8]

The silica nanoparticles are among the most widely used additives and fillers for polymer materials. Because of the high hydrophilicity of silica and hydrophobic nature of most organic polymers, it is a big challenge to produce polymer/silica composites with homogeneous particle distribution. The existing recipes for the polymer/silica composite preparation such as mixing in solution or melt, as well as solution sol−gel technology, either require a large amount of solvent or lead to significant particle agglomeration. Recently, we proposed a new route for preparation of polymer/silica composites, which is compatible with industrial fabrication.[9] The process is based on a solvent-free *in situ* sol−gel technology employing a nonvolatile silica precursor polymer: hyperbranched polyethoxysiloxane (PEOS).[10,11] By following this route, the isotactic polypropylene (iPP)/silica composites were prepared in a twin-screw mini-extruder. According to transmission electron microscopy (TEM) data, for small amounts of PEOS (≤5 wt %) the procedure yields iPP/silica composites with particles smaller than 100 nm. For higher PEOS loadings, the particle size increases up to several micrometers. Importantly, the *in situ* generated nano- or microparticles are homogeneously dispersed within the polymer matrix.[9]

Generally, injection molding is one of the most common processing techniques for the semicrystalline iPP.[12] In the course of injection molding, iPP undergoes flow-induced crystallization. The presence of additives can have a strong influence on this process and eventually affect the final morphology and properties of the resulting articles.[13] Recently, a combination of differential scanning calorimetry (DSC), small- and wide-angle X-ray scattering (SAXS/WAXS), and ^{1}H time-domain and frequency-domain nuclear magnetic resonance (NMR) measurements was employed to determine the rigid (crystalline), semirigid (interface), and mobile (amorphous) fractions in semicrystalline iPP as a function of annealing time and temperature.[14] The data on the iPP microstructure provided by proton spin-diffusion NMR[15] and SAXS allow to address the effect of annealing,[14] uniaxial stretching, and aging.[16,17] Solid-state NMR is a powerful technique for investigation of morphology and chain dynamics of polymer materials.[15,18−20] The phase composition and size of different structural domains can be conventionally determined based on the wide-line NMR spectra and spin-diffusion measurements, respectively. In comparison to X-ray scattering, NMR can

---

*To whom correspondence should be addressed: tel +49-241-80-23341, fax +49-241-80-23301, e-mail zhu@dwi.rwth-aachen.de (X.Z.); tel +33-389608807, fax +33-389608799, e-mail dimitri.ivanov@uha.fr (D.A.I.).

© 2010 American Chemical Society

Published on Web 06/14/2010

provide additional information on the intermediate phase between the rigid and mobile fractions associated with the semicrystalline lamellar structure.[21−24] The interface region is characterized by a degree of order in the direction perpendicular to the basal lamellae surface along with disorder in the lateral direction and is one of the key factors determining the overall morphology and the mechanical properties of semicrystalline polymers.

The aim of this work is to study the impact of the *in situ* formed silica particles on the structure formation in the iPP/silica composites during the injection molding process and to establish correlations between the morphology of the injection-molded articles and their rheological and mechanical properties. To determine the degree of crystallinity, phase composition and domain size the SAXS/WAXS and ^{1}H solid-state NMR are employed. The gradient of the chain dynamics at the rigid/mobile interfaces in the iPP/silica composites is measured by the ^{1}H spin-diffusion experiment.

2. Experimental Section

Sample Preparation. The details of the sample preparation procedure were reported elsewhere.[9] A commercial isotactic polypropylene grade (iPP, Basell Moplen HF500N) was used to fabricate iPP/silica composites. The resulting composites were processed on a 5.5 mL injection molding machine (DSM Xplore) into standard specimens for tensile testing with gauge length of 20 mm, width of 4 mm, and thickness of 2 mm (ISO 527-2 5A) under the following conditions: cylinder temperature 200 °C, mold temperature 60 °C, holding pressure 7 MPa, holding time 12 s, and cooling time 20 s. For rheological measurements, disks of 25 mm diameter and 1 mm thickness were injection-molded under the same conditions.

Small- and Wide-Angle X-ray Scattering (SAXS/WAXS). X-ray scattering experiments were performed on a custom-built SAXS/WAXS machine coupled to a Rigaku MicroMax-007 HF rotating anode generator ($\lambda = 1.54$ Å). The size of the pointlike X-ray beam on the sample was ~300 μm. The 2D WAXS data were collected using X-ray-sensitive Fuji image plates with the pixel size of 100 × 100 μm^2. SAXS data were recorded with a 2D multiwire detector. The modulus of the scattering vector s ($s = 2 \sin \theta/\lambda$, where θ is the Bragg angle) was calibrated using three diffraction orders of silver behenate. The hole in the center of the image plate allows performing simultaneous SAXS and WAXS measurements.

For X-ray diffraction measurements small pieces of iPP composites were cut out from the central part of standard specimens for tensile testing as depicted in Figure 1. The skin layers parallel to the machine direction (MD) and perpendicular to the transverse direction (TD) were removed from the two faces.

The diffraction patterns of pure iPP showed only reflections pertinent to the α-phase, whereas the iPP composites also revealed the presence of β-crystals. The experimental Lorenz-corrected WAXS curves were fitted with a sum of Gaussian functions (cf. Figure 2) corresponding to the crystalline peaks and the amorphous halo. To calculate the relative content of each crystalline phase, the total area of the most intense peaks such as the 110, 040, 130, 111, $1\bar{3}1$/041, 150, 060, and 220 for the α-phase and 300 and 311 for the β-phase were normalized by the total intensity. Since the amorphous halo of the composite samples contains the contribution from amorphous silica, its intensity was renormalized by the iPP fraction.

The 3D morphology of the injection-molded iPP is known to contain the "shish-kebab"-like primary skeleton structures with the axis parallel to MD, which are piled epitaxially with the a*-axis-oriented lamellar substructure or the so-called "daughter" crystals.[25] In this work, the orientation factor of the α-phase "mother" crystals was calculated from the P_2 Legendre polynomial function:

$$f = \frac{3\langle \cos^2 \phi \rangle - 1}{2} \tag{1}$$

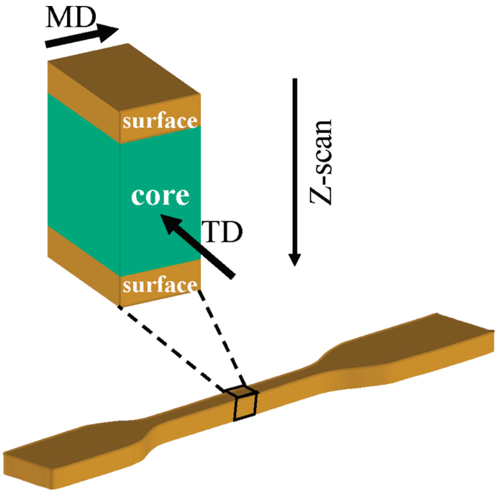

Figure 1. Injection-molded iPP/silica specimen showing the central part cut out from it for SAXS/WAXS measurements. The MD and TD stand for the machine and transverse direction, respectively.

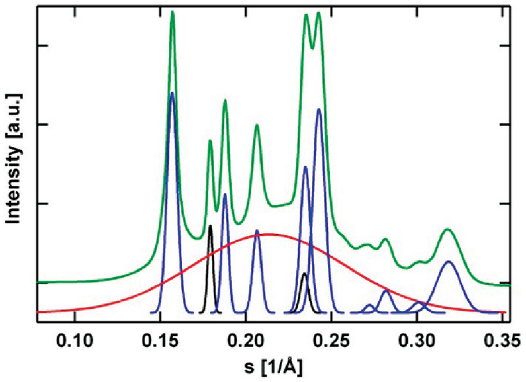

Figure 2. Example of diffraction peak decomposition for an iPP/silica composite with 7.5 wt % of PEOS. The experimental curve (green) was fitted with a sum of Gaussian peaks representing the amorphous halo (red curve) and crystalline peaks of the α- and β-phase (blue and black curves, respectively).

To this end, the 110 peak intensity was azimuthally integrated with the corresponding factor the in the ϕ-range from 0 to $\pi/4$ to exclude the contribution from the "daughter" crystals. Here ϕ stands for the angle of the "daughter" crystals peak with respect to the equatorial direction. The relative content of the α-phase "daughter" crystals w was calculated from the azimuthally integrated intensities of the 110 reflection I_1 and I_2 corresponding to the "mother" and "daughter" lamellae:

$$w = \frac{I_2(\phi) \cos \phi}{I_1(0)} \tag{2}$$

The cosine correction was neglected for the orientation factor calculation due to the small angular spread of the 110 peak about the equator.

The thickness of the amorphous (L_a) and crystalline (L_c) domains as well as long period ($LB \equiv L_a + L_c$) were calculated from the conventional SAXS interface distribution functions (IDF).[26,27] The microstructural analysis based on these functions is illustrated in Figure 3. In this case, the values of LB are computed from the first minimum of the IDF whereas the thickness distributions corresponding to L_c and L_a can be discriminated from the behavior of IDF close to the origin. However, the attribution of the distances cannot be made from the SAXS data alone due to the Babinet principle and therefore requires additional structural information such as the bulk crystallinity determined from WAXS or DSC.[28−30]

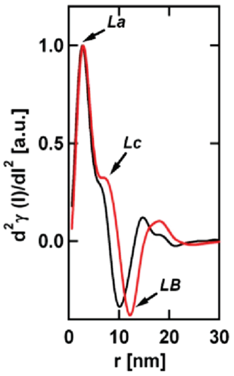

Figure 3. Interface distribution functions computed from 1D SAXS patterns for pure iPP (black) and iPP composite with 20 wt % PEOS (red).

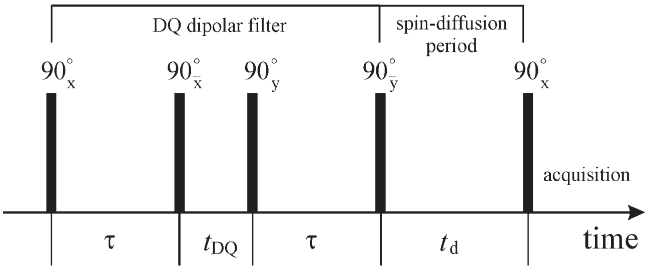

Figure 4. Scheme of the pulse sequence used for the proton spin-diffusion experiment. The first two pulses excite double-quantum (DQ) coherences and have a duration τ. The following time interval is very short, corresponding to the DQ coherences free evolution. The next two pulses reconvert DQ coherences in z-magnetization. The last pulse is used for editing the NMR signal.

Solid-State NMR Measurements and Data Analysis. Two ^{1}H solid-state NMR methods were used to characterize the injection-molded iPP/silica composite articles; these are ^{1}H wide-line NMR spectra and ^{1}H spin-diffusion NMR. All NMR measurements were conducted with a Bruker DSX spectrometer operating at a proton resonance frequency of 500.45 MHz. The data were collected for static samples at 25 °C, which is above the glass transition temperature of iPP. This provided high contrast in the NMR experiments to discriminate the chain mobility of different regions. The duration of the 90° pulse was about 5 μs, and the dwell time was set to 1 μs. A recycle delay of 5 s was used in all cases. The dead time of the spectrometer is 5.5 μs.

Proton NMR spin-diffusion measurements were performed following the general scheme, which consists of a double-quantum (DQ) dipolar filter, a spin-diffusion period, and an acquisition period (Figure 4).[31−35] A magnetization gradient was created by the dipolar filter that excites DQ coherences and selects mainly the magnetization of the rigid phase. This type of filter is more advantageous to use than a dipolar filter for the mobile domains because the DQ filter allows a more accurate detection of the narrow line growing on the top of the broad one as compared to the detection of the broad line forming under the narrow signal. This is valid especially at short spin diffusion times when the intensity of one of the components is very small. The pulse sequence is based on two pulses acting during both the excitation and the reconversion periods (Figure 4). The value of the excitation/reconversion time τ is 7 μs. It corresponds to the rising region of the DQ build-up curve for each sample. The evolution time of the DQ coherences was set to 5 μs.

For NMR studies the samples were cut from the central part of the tensile test specimens as depicted in Figure 1, and then a skin layer of 0.5 mm was removed from all four faces. The resulting piece was cut into small grains, which were placed into a 4 mm MAS rotor.

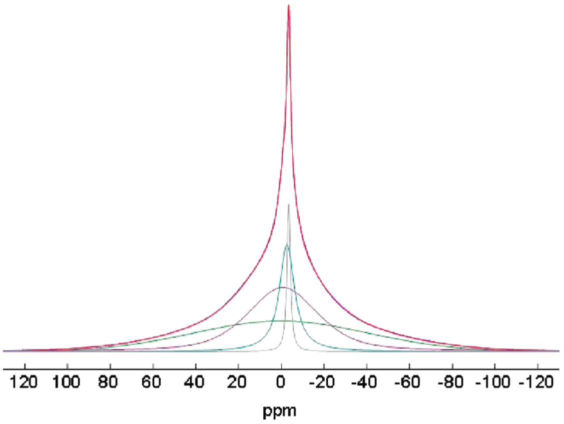

Figure 5. Proton wide-line NMR spectrum of iPP with 20 wt % PEOS, measured at room temperature. The spectra are decomposed into four components. The narrowest component in the spectrum is associated with the very mobile protons of remaining ethoxy groups. The other lines show the spectral components that are assigned to the rigid, semirigid, and soft fractions of iPP, with broad, intermediate, and narrow line widths, respectively.

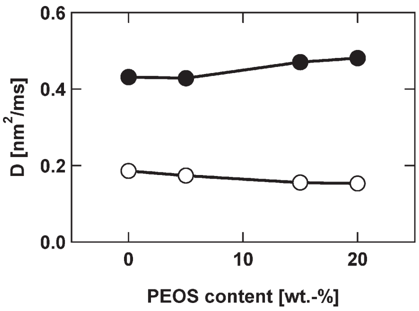

Figure 6. Spin diffusivities for the rigid (full circles) and amorphous (empty circles) fractions of iPP with different PEOS loadings.

Proton wide-line NMR spectra were decomposed into four components using the DMFIT program (Figure 5). The broad component of the spectra was approximated by a Gaussian function. The shape of the line with intermediate width (i.e., the interface) was fitted using a combination of Gaussian and Lorentzian functions. The narrow component of the spectra, which belongs to the amorphous fraction with high chain mobility, can be well described by a Lorentzian function. This is also valid for the very narrow component (~1 kHz) that is related to the fast-moving protons of the remaining ethoxy groups on the silica particles.

Proton spin diffusivities were calculated using a literature procedure.[31] The values of the spin-diffusivities D_R and D_M for the rigid and mobile fractions, respectively, can be determined by approximating the NMR line shapes of the rigid and the mobile fractions by Gaussian and Lorentzian functions, respectively. The weak dependence of the spin diffusion coefficients of iPP on the PEOS content is shown in Figure 6.

Since the conventional cross-hatched morphology of the α-phase crystals was observed in all studied samples by means of 2D WAXS, the spin-diffusion process was approximated by a 2D square-transverse morphology. The thickness of the rigid and mobile domains was obtained from the solution of the spin-diffusion equations and the decay and buildup experimental curves as described previously.[31−33]

Rheological Investigation. The rheological study was performed using a cone−plate rheometer of type DSR SR-200 (Rheo service, Reichelsheim, Germany) equipped with electrically heated parallel plates (Φ = 25 mm, gap ~1.0 mm for all samples). The measurement was carried out at 200 ± 0.1 °C in the range of shear rates from 0.1 to 100 s^{-1}.

Size Exclusion Chromatography (SEC). The samples for SEC were cut out from the injection-molded articles. SEC analyses were conducted at 150 °C with a differential refractive index detector and a four-capillary differential viscometer detector. The eluting solvent was 1,2,4-trichlorobenzene. The molecular weight of the polymer was determined using universal calibration.

3. Results and Discussion

The iPP/silica composites studied in this work were prepared by means of *in situ* sol−gel technology, in which a volatile-free silica precursor, hyperbranched polyethoxysiloxane (PEOS), was converted to solid silica by water vapor in the iPP melt.[9] According to TEM micrographs, the sample prepared with a small amount of PEOS (5 wt %) contained silica particles of 30−40 nm in size. However, due to incompatibility of PEOS with PP, the particle size increased when more PEOS was added. With the PEOS content of 10 wt %, particles of 300−400 nm in size were observed. At relatively high loading of PEOS (15−20 wt %), silica particles of several micrometers were formed. It is noteworthy that, despite the particle size variation, the volume distribution of the particles remains rather homogeneous.[9]

After synthesis in a twin-screw extruder, the iPP/silica composites were immediately processed to fabricate standard specimens for tensile tests. According to high-temperature size exclusion chromatography (SEC), the molecular weights of iPP as well as weight distribution were not affected by this processing. We found that at low silica contents the Young's modulus was somewhat smaller in comparison with that of pure iPP. However, with further increase of silica loading it increased slightly and became similar to that of the pure polymer.[9]

It is well documented that injection-molded samples of iPP have a "core−skin" structure.[36] The "skin" is characterized by a relatively high amorphous content due to its thermal quenching produced by the thermal contact with cold metal walls of the mold. In the inner ("core") layer, the comparatively lower cooling rate allows for a more complete loss of the chain orientation, which in turn results in isotropic spherulitic growth. The skin and core zones are separated by a "shear zone" whose structure is characterized by the presence of row-nucleated spherulites, which are typical of crystallization from the oriented melt. To study the effect of shearing force distribution on the semicrystalline structure, the spatially resolved WAXS patterns were recorded with the X-ray beam oriented along the transverse direction (cf. the sketch in Figure 1). Figure 7 shows typical angular distributions of the 110 peak intensity of the α-crystals across the whole sample thickness. As expected, all the samples display a well-oriented crystalline structure in the outer layer. As far as orientation in the sample core is concerned, the sample of pure iPP is largely isotropic (Figure 7a). By contrast, the core of the iPP/silica composite shown in the figure does show orientation (Figure 7b), although it is not as pronounced as that in the surface layer of the same sample.

To get a better idea of the sample texture, it is instructive to compare the 2D WAXS patterns resulting from the core of pure iPP and from one typical composite specimen (Figure 8). It can be clearly seen that, in contrast to pure iPP, the composite sample shows a well-pronounced crystal orientation. From the analysis of the diffraction peak positions and integrated peak intensities the crystal phase composition in the core and surface layer of the samples was determined (cf. Figure 9). In the pure iPP sample only the peaks of the α-phase were observed, whereas the α- and *β*-phases coexist in the composite samples. In the surface layer, the α/*β* ratio slightly increases with the PEOS loading. However, in the sample core, the opposite trend was observed. The content of the *β*-phase in the surface layer is negligibly small. In the

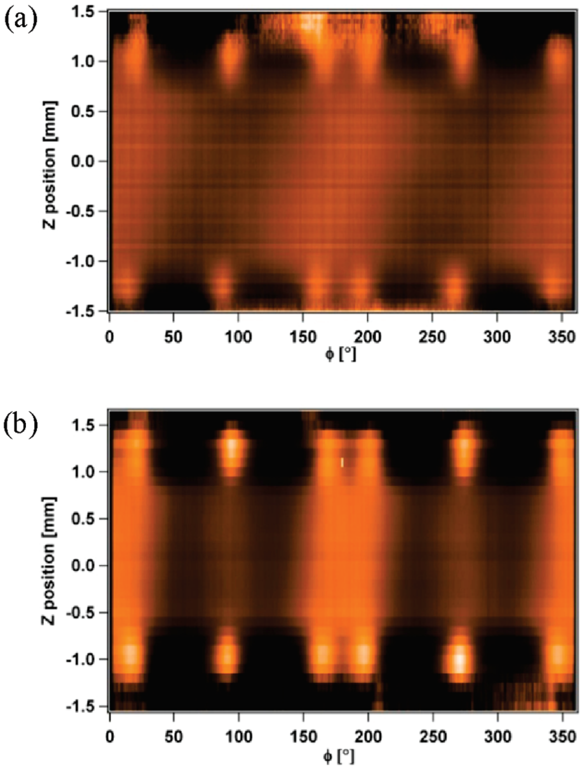

Figure 7. Azimuthal distribution of the 110 peak intensity across the whole injection-molded specimen thickness (*Z*-position): (a) pure iPP; (b) iPP/silica composite loaded with 7.5 wt % PEOS.

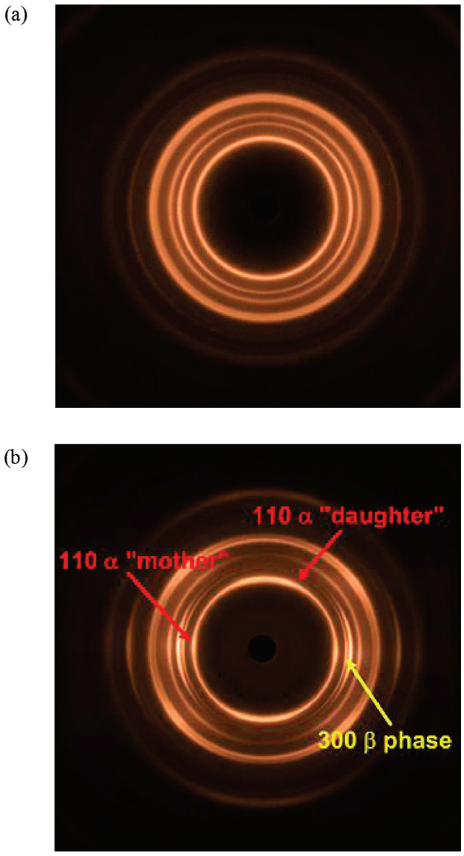

Figure 8. 2D WAXS patterns measured on the core of the pure iPP (a) and iPP/silica composite loaded with 20 wt % PEOS (b). The machine direction (MD) is vertical.

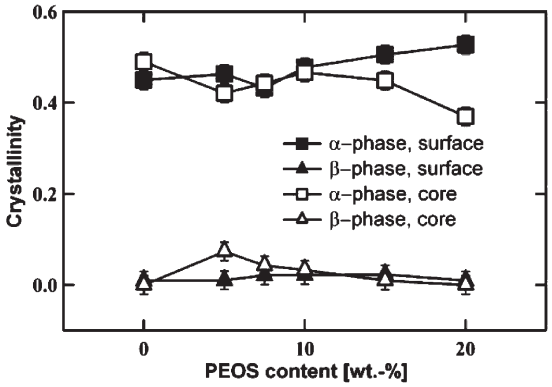

Figure 9. Contents of different crystalline phases of iPP composite samples as a function of PEOS loading.

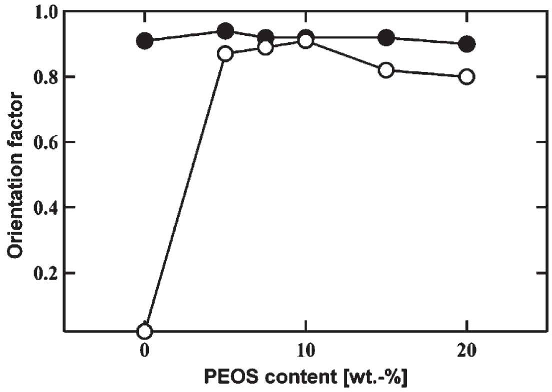

Figure 10. Orientation factor *f* of the primary α-crystals in surface layer (solid circles) and sample core (empty circles) as a function of PEOS loading.

sample core, the highest content of 8% was found at 5 wt % PEOS loading. Upon further increase of PEOS the amount of the β-phase starts to decrease. Therefore, at low PEOS loadings (<10 wt %) the *in situ* generated nanosized silica particles serve as β-nucleating agent. The increase of the silica particle size occurring at higher loadings probably result in the loss of their nucleating efficiency.

Two orientations of the α-crystals can be observed in the 2D WAXD pattern corresponding to the core of the iPP composite samples (Figure 7b). As in the classical picture of the iPP morphology formed during injection molding,[25] the chains pertinent to the primary ("mother") crystals are aligned along the flow direction. The chains of the secondary crystal fraction ("daughter" crystals) are oriented almost normal to the flow direction. The 110 and 130 peaks from the "daughter" crystals were found to be inclined at 15° and 43° away from the meridian, respectively. The coexistence of these two crystal populations as well as their higher order derivatives such as "granddaughter" form the conventional "cross-hatched" or "notch-divider" morphology.[37] To quantify the degree of orientation, the orientation factor *f* of the primary α-crystals was computed by azimuthally integrating the 110 reflection intensity (Figure 10). In the surface layer of the pure iPP and composite samples the primary crystals are found to be highly oriented, the orientation being almost independent of the PEOS loading. However, a different trend is observed for the sample core. By loading the polymer matrix even with a small amount of silica particles, the orientation factor rapidly increases to values above 0.8 (cf. Figure 10). At high silica contents it slightly decreases again, which can be accounted for by a decrease of specific interface between the particles and polymer matrix.

Table 1. Fraction of "Daughter" Crystals Calculated from Azimuthal Intensity Distribution of the 110 Peak (See Text for More Details)

PEOS content, wt %	fraction of "daughter" crystals
0	0.12
5	0.37
7.5	0.41
15	0.39
20	0.41

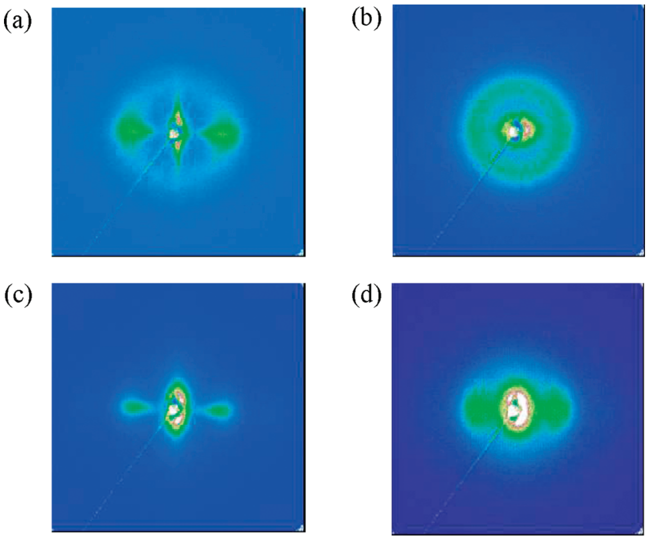

Figure 11. 2D SAXS patterns corresponding to the skin (a, c) and core (b, d) of the pure iPP sample and iPP composite loaded with 20 wt % PEOS, respectively. The machine direction is horizontal.

As mentioned above, two orientations of the α-phase, namely "mother" and "daughter" crystals, are clearly discriminated in the core of the injection-molded samples. The analysis of the azimuthal intensity distributions indicates that the relative content of the "daughter" crystals drastically increases with incorporation of the *in situ* generated silica particles from 12% for pure iPP to 37% for the iPP composite with 5 wt % of PEOS (cf. Table 1). Upon further increase of the PEOS content, the fraction of the "daughter" crystals does not change significantly (cf. Table 1). Since the "mother" crystals determine the mechanical strength in the machine direction, a decrease of their amount can result in a decrease of the MD Young's modulus. At high silica contents this effect is probably compensated by the contribution coming from the silica particles. This effect is likely to explain the V-shaped dependence of the Young's modulus on the PEOS loading reported previously.[9]

To analyze the crystalline lamellae arrangement in the injection-molded iPP samples, 2D SAXS measurements have been conducted. Figure 11 shows the SAXS patterns recorded on both surface and core zones of the samples. Similar to the WAXS results presented above, the "mother" lamellae in the surface layer stay always oriented, being independent from the silica fraction. It should be noted that the vertical streak in small-angle region on the SAXS pattern of pure iPP (Figure 11a) is typical of the extended chain crystals or the so-called "shishes".[38,39] For the composites the streak is hidden by strong scattering from the silica particles. Therefore, the role of these particles on the formation of the "shish" scaffold still has to be clarified.

In the sample core, pronounced orientation of the crystalline lamellae was observed only for the iPP/silica composites. Despite a significant fraction of the "daughter" crystals in the composite samples, no interference maxima in the vertical direction of the 2D SAXS patterns, i.e., the one perpendicular to MD, were detected. This indicates the absence of a regular stacking of the

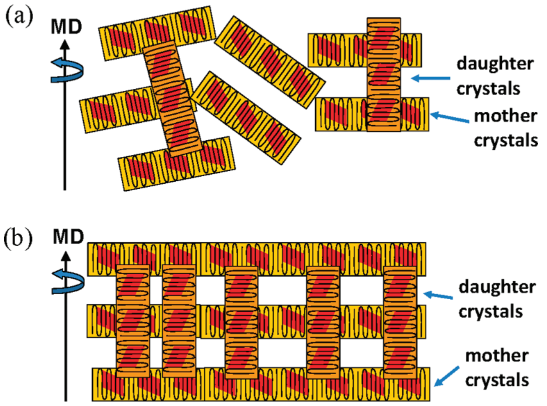

Figure 12. Schematic representation of the lamellar arrangement in the core of pure iPP sample (a) and iPP/silica composites (b). The sketch shows an improvement of the "mother" lamellae orientation and increase of the "daughter" crystal fraction with addition of the silica particles to the iPP matrix.

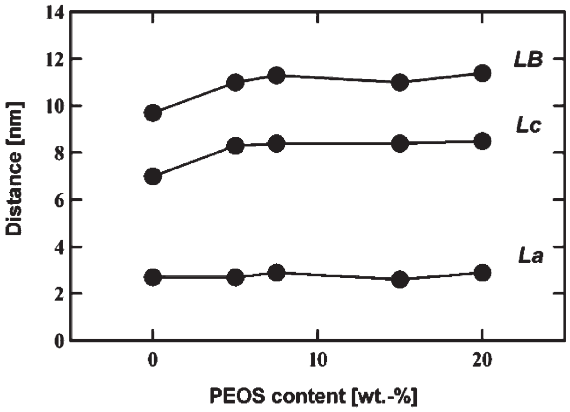

Figure 13. Dependence of the amorphous layer thickness L_a, crystal thickness L_c, and long period *LB* on the PEOS content calculated from the SAXS interface distribution function.

"daughter" lamellae. Figure 12 sketches the lamellae ordering in the core of the pure iPP sample and iPP/silica composites.

The thickness of the amorphous (L_a) and crystalline (L_c) domains and the long period (*LB*) were calculated from the 1D SAXS curves using the interface distribution functions (Figure 3). The dependence of these parameters on the PEOS loading is shown in Figure 13. It was found that the thickness of the smallest region, i.e., the interlamellar amorphous layer, is ca. 2.6 nm and does not show any significant changes when varying the silica particles fraction. By contrast, the largest distance, i.e., the crystal thickness, significantly increases when silica particles are added: it grows from 7.0 nm for pure iPP to 8.2 nm for the composite with 5 wt % PEOS. Upon further increase of the filler fraction, the crystal thickness remains almost constant. The assignment of the two SAXS distances was chosen to be compatible with the bulk crystallinity values determined from WAXS (cf. Figure 9).

For more information on the phase composition ^{1}H wide-line NMR spectra in the static regime were recorded and subsequently decomposed into four components. From such decomposed spectra the fractions of rigid (crystalline), semirigid (interfacial), and mobile (amorphous) parts of iPP can be obtained as a function of PEOS loading; the result is shown in Figure 14. It should be noted that the rigid fraction determined from ^{1}H wide-line NMR spectra is quite close to the crystallinity measured by WAXS. At the same time the dependence of the rigid fraction/crystallinity on the PEOS loading obtained by these two techniques shows a similar trend; i.e. it decreases with the increase of PEOS content, and the most significant change is observed in the range from 0 to 5 wt %. The semirigid and mobile fractions, however, increase with the increase of the PEOS loading. The latter is understandable since the silica particles are localized in the amorphous and interfacial regions.

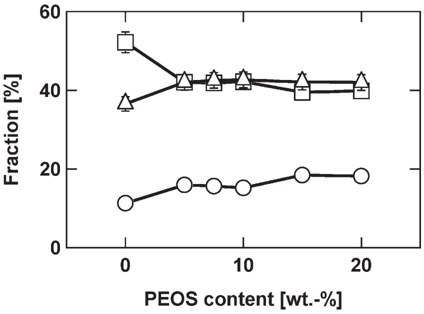

Figure 14. Amounts of rigid (squares), semirigid (triangles), and mobile (circles) fractions of iPP as a function of PEOS content measured from ^{1}H wide-line NMR spectra.

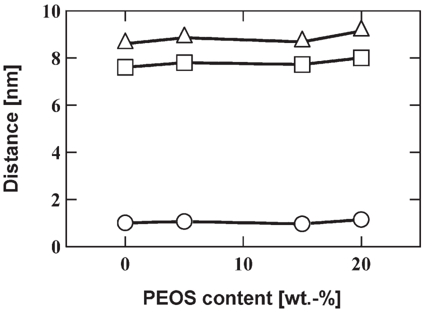

Figure 15. Rigid (squares) and mobile (circles) domain thickness and long period (triangles) of iPP versus PEOS content.

The decay and build-up spin-diffusion curves for pure iPP and iPP/silica composites were measured by the pulse sequence shown in Figure 4. The thickness of the rigid L_r and soft L_m domains in these samples was determined by fitting the dependencies of the signal integrals of these fractions as a function of the spin-diffusion time. For this purpose a 2D analytical solution for the spin-diffusion equations was used.[31,34] The values of the spin diffusivities present in the solution of the spin-diffusion equations for the rigid and soft fractions of the iPP composites are shown in Figure 6. The long period $LB \equiv L_r + L_m$ of the iPP lamellae can be obtained from the experimentally determined values of L_r and L_m. The dependence of the domain thicknesses and the long period on the PEOS content is shown in Figure 15. The domain thicknesses determined by both SAXS and NMR spin-diffusion techniques are quite close and show similar dependences on the PEOS content, i.e., a slight increase in the thickness of the rigid domain by adding small amount of silica. The small difference in the absolute values is due to the different physical contrast in SAXS and NMR methods.

Proton spin-diffusion experiment using a DQ filter allows us to measure the spatial evolution of the *z*-magnetization front by the spectral decomposition. At the beginning of the spin-diffusion experiment the magnetization is stored only in the rigid domain. For short spin-diffusion time the magnetization is present in the rigid and interface domains. At longer diffusion times the *z*-magnetization front will reach the mobile region by spatially evolving until the thermodynamic quasi-equilibrium is achieved. The interfacial region has a gradient in molecular mobility, and therefore a monotonic change in the line width at the half-intensity ($\Delta\nu_{1/2}$) can be detected. At shorter spin-diffusion time the experiment edits the part of the interface closer to rigid region.

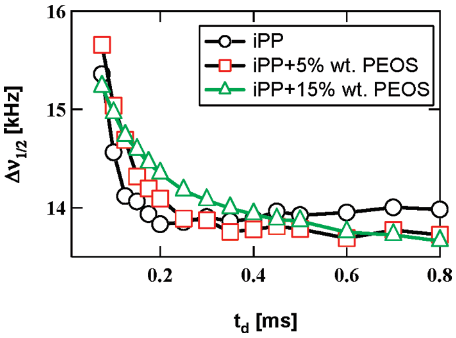

Figure 16. Full line width at the half-intensity ($\Delta\nu_{1/2}$) of the interfacial spectral component of the ^{1}H NMR spectrum for iPP with different contents of PEOS as a function of spin-diffusion time t_d.

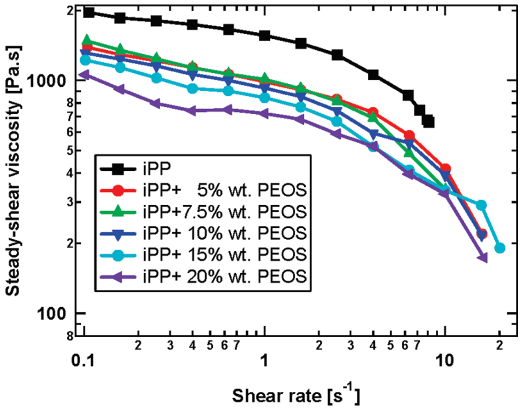

Figure 17. Steady-shear viscosity versus shearing rate at 200 °C for pure iPP and iPP/silica composites.

For longer diffusion time the most mobile part of the interface connected to the mobile region will be edited. The gradual change in the line width at the half-intensity of the interface spectral component is shown in Figure 16 for pure iPP and iPP with 5 and 15 wt % PEOS. The sharpest gradient in the molecular mobility is detected for the pure iPP. The chain mobility at the interface undergoes some change with a gentler slope for the samples with silica particles. It seems that by addition of silica particles the interface between the rigid and soft parts becomes more diffused. It should be specially mentioned that in the soft (amorphous) domains the polymer chains are more mobile in the presence of silica particles, which is reflected by a smaller line width at half-intensity (Figure 16). This result coincides with the tensile testing data, which showed a decrease of strain hardening modulus during stretching at high strains by silica incorporation.[9]

Above we have discussed on the morphology of the iPP composites filled with different amounts of the *in situ* formed silica particles. It was observed that incorporation of the silica particles results in improved orientation of the "mother" crystals, reduction of the "mother" crystal fraction, and crystal thickening. The observed variation of the particle−matrix interphase can be also addressed by rheological measurements. In Figure 17 we compare the rheology of the iPP/silica composites with that of pure iPP. It can be seen that the viscosity of iPP is reduced by addition of the silica particles. The biggest drop in viscosity was observed in the PEOS range from 0 to 5 wt %, whereas further increase of PEOS content led only to a slight reduction. The silica particles formed in the iPP are pretty big ranging from tens of nanometers to several micrometers, so the effect of these particles is in contradiction with conclusions made by Mackay et al., who reported that the viscosity of the polymer melt can be reduced only in the case when the interparticle half-gap is smaller than the radius of gyration of the polymer coil.[6] The incompatibility of the *in situ* formed silica particles with the iPP matrix together with homogeneous volume distribution might be the reason for such an effect.

As previously shown by us, the *in situ* generated silica particles behave as a weak nucleator by increasing the crystallization temperature of iPP for about 5 °C.[9] It is known that addition of nucleating agents to the iPP matrix can also change the structure of injection-molded specimens; e.g., it can enhance the orientation degree of crystals due to incomplete relaxation of the melt orientation (recoverable shear strain)[40−42] and increase the lamellar thickness.[43] It means that the crystal nucleation by the silica particles can contribute to these two phenomena observed in the core zone of the iPP/silica composite samples, although the nucleating effect is pretty weak. The increase of the "daughter" crystal fraction by the silica inclusion can be probably merely attributed to the reduction of the melt viscosity due to the increased rate of the polymer coil relaxation. Thus, it was reported that the increase of the cylinder temperature led to a higher "daughter" crystal fraction.[41] The elevation of the cylinder temperature can decrease the melt viscosity; the silica particles have the same effect in our case. In addition, we have found that the β-crystals are formed mainly in the core zone of the composite samples; this is in contrast to previous results obtained on injection-molded samples of iPP filled with nucleating agents, where the formation of β-crystals was observed only in the surface layer,[40−42] since their formation was promoted by shear. This can possibly be the result of the reduced melt viscosity in the composite samples.

4. Conclusions

A combination of wide- and small-angle X-ray scattering and solid-state NMR spectroscopy was used to analyze the semicrystalline morphology of injection-molded isotactic polypropylene (iPP)/silica composites prepared via *in situ* sol−gel technology using hyperbranched polyethoxysiloxane (PEOS) as the silica precursor. The results regarding the phase composition and lamellar microstructure obtained from both X-ray and NMR techniques are quite close. By means of WAXS it was demonstrated that the "mother" crystal fraction was largely decreased by incorporation of the *in situ* formed silica particles. This fact together with the solid filler effect can be the reason for the observed V-shaped dependence of Young's modulus of the composites on the PEOS loading. Both WAXS and SAXS revealed a significant orientation of the iPP crystals in the core of the injection-molded parts in the machine direction; meanwhile, the core of the pure iPP sample did not exhibit any orientation. The β-crystals were formed in the core zone of the iPP/silica composite samples, and their maximal amount was observed at the PEOS content of 5 wt %. In contrast to previous results obtained on injection-molded samples of iPP filled with nucleating agents, where the formation of β-crystals was observed only in the surface layer, in this work it has been found that the β-crystals are formed mainly in the core zone of the composite samples. All these phenomena are most probably due to the nucleating effect as well as to a decrease of the polymer melt viscosity by the silica particles, which was demonstrated by the rheological measurements. Proton spin-diffusion experiment using a double quantum filter was proved to be a suitable method to measure chain mobility gradient in the interface region, and it indicated as well the increase of the polymer chain mobility in the amorphous region in the presence of silica particles. The latter result coincided with the tensile testing data, which showed a decrease of strain hardening modulus during stretching at high strains by the silica inclusion.

Acknowledgment. The financial support of the Deutsche Forschungsgemeinschaft (ProjectMO682/12-1) and L'Agence Nationale de la Recherche project SPIR-Wind (N 08-HABI-SOL-014-04) is gratefully acknowledged.

References and Notes

(1) *Functional Fillers for Plastics*; Xantos, M., Ed.; Wiley-VCH: Weinheim, 2005.

(2) *Polymer Composites - From Nano to Macro-scale*; Friedrich, K., Fakirov, S., Zhang, Z., Eds.; Springer Science+Business Media, Inc.: New York, 2005.

(3) Koo, J. H. *Polymer Nanocomposites - Processing, Characterization, and Applications*; McGraw-Hill: New York, 2006.

(4) Einstein, A. *Ann. Phys.* (*Leipzig*) **1906**, *19*, 371–381.

(5) Mackay, M. E.; Dao, T. T.; Tuteja, A.; Ho, D. L.; Van Horn, B.; Kim, H.-C.; Hawker, C. J. *Nature Mater.* **2003**, *2*, 762–766.

(6) Tuteja, A.; Mackay, M. E.; Hawker, C. J.; Van Horn, B. *Macromolecules* **2005**, *38*, 8000–8011.

(7) Tuteja, A.; Duxbury, P. M.; Mackay, M. E. *Macromolecules* **2007**, *40*, 9427–9434.

(8) Tuteja, A.; Mackay, M. E.; Narayanan, S.; Asokan, S.; Wong, M. S. *Nano Lett.* **2007**, *7*, 1276–1281.

(9) Dou, Q.; Zhu, X.-M.; Peter, K.; Demco, D. E.; Möller, M.; Melian, C. *J. Sol-Gel Sci. Technol.* **2008**, *48*, 51–60.

(10) Jaumann, M.; Rebrov, E. A.; Kazakova, V. V.; Muzafarov, A. M.; Goedel, W. A.; Möller, M. *Macromol. Chem. Phys.* **2003**, *204*, 1014–1026.

(11) Zhu, X.-M.; Jaumann, M.; Peter, K.; Möller, M.; Melian, C.; Adams-Buda, A.; Demco, D. E.; Blümich, B. *Macromolecules* **2006**, *39*, 1701–1708.

(12) *Handbook of Polypropylene and Polypropylene Composites*, 2nd ed., revised and expanded; Karian, H. G., Ed.; Marcel Dekker: New York, 2003.

(13) Hwang, W. R.; Peters, G. W. M.; Hulsen, M. A.; Meijer, H. E. H. *Macromolecules* **2006**, *39*, 8389–8398.

(14) Hedesiu, C.; Demco, D. E.; Kleppinger, R.; Vanden Poel, G.; Gijsbers, W.; Blümich, B.; Remerie, K.; Litvinov, V. M. *Macromolecules* **2007**, *40*, 3977–3989.

(15) Schmidt-Rohr, K.; Spiess, H. W. *Multidimensional Solid-State NMR and Polymers*; Academic Press: London, 1994.

(16) Hedesiu, C.; Demco, D. E.; Remerie, K.; Blümich, B.; Litvinov, V. M. *Macromol. Chem. Phys.* **2008**, *209*, 734–745.

(17) Hedesiu, C.; Demco, D. E.; Kleppinger, R.; Vanden Poel, G.; Remerie, K.; Litvinov, V. M.; Blümich, B.; Steenbakkers, R. *Macromol. Mater. Eng.* **2008**, *293*, 847–857.

(18) Bovay, F. A.; Mirau, P. A. *NMR of Polymers*; Academic Press: San Diego, 1996.

(19) *Solid State NMR of Polymers, Studies in Physical and Theoretical Chemistry 84*; Ando, I., Asakura, T., Eds.; Elsevier: Amsterdam, 1998.

(20) Hatada, K.; Kitayama, T. *NMR Spectroscopy of Polymers*; Springer-Verlag: Berlin, 2004.

(21) Tanaka, H.; Kohrogi, F.; Suzuki, K. *Eur. Polym. J.* **1989**, *25*, 449–453.

(22) Dadayli, D.; Harris, R. K.; Kenwright, A. M.; Say, B. J.; Sünnetçioglu, M. M. *Polymer* **1994**, *35*, 4083–4087.

(23) Schreurs, S.; Francois, J. P.; Adriaenens, P.; Gelan, J. *J. Phys. Chem. B* **1999**, *103*, 1393–1401.

(24) Tanaka, H.; Inoue, Y. *Polym. Int.* **1993**, *31*, 9–13.

(25) Fujiyama, M.; Wakino, T.; Kawasaki, Y. *J. Appl. Polym. Sci.* **1988**, *35*, 29–49.

(26) Ruland, W. *Colloid Polym. Sci.* **1977**, *255*, 417–427.

(27) Balta-Calleja, F. J.; Vonk, C. G. *X-ray Scattering of Synthetic Polymers*; Elsevier: Amsterdam, 1989.

(28) Ivanov, D. A.; Legras, R.; Jonas, A. M. *Macromolecules* **1999**, *32*, 1582–1592.

(29) Ivanov, D. A.; Amalou, Z.; Magonov, S. N. *Macromolecules* **2001**, *34*, 8944–8952.

(30) Ivanov, D. A.; Bar, G.; Dosière, M.; Koch, M. H. J. *Macromolecules* **2008**, *41*, 9224–9233.

(31) Demco, D. E.; Johansson, A.; Tegenfeldt, J. *Solid State Nucl. Magn. Reson.* **1995**, *4*, 13–38.

(32) Buda, A.; Demco, D. E.; Bertmer, M.; Blümich, B.; Litvinov, V. M.; Penning, J. P. *J. Phys. Chem. B* **2003**, *107*, 5357–5370.

(33) Buda, A.; Demco, D. E.; Blümich, B.; Litvinov, V. M.; Penning, J. P. *ChemPhysChem* **2004**, *5*, 876–883.

(34) Buda, A.; Demco, D. E.; Bertmer, M.; Blümich, B.; Reining, B.; Keul, H.; Höcker, H. *Solid State Nucl. Magn. Reson.* **2003**, *24*, 39–67.

(35) Voda, A. M.; Demco, D. E.; Voda, A.; Schauber, T.; Adler, M.; Dabisch, T.; Adams, A.; Baias, M.; Blümich, B. *Macromolecules* **2006**, *39*, 4802–4810.

(36) Tronignon, J.-P.; Verdu, J. In *Interrelationships between Processed Structures and Properties of Polymer Materials*; Seferis, J. C., Theocaris, P. S., Eds.; Elsevier: New York, 1984; p 471.

(37) Padden, F. J.; Keith, H. D. *J. Appl. Phys.* **1966**, *37*, 4013–4020.

(38) Kimata, S.; Sakurai, T.; Nozue, Y.; Kasahara, T.; Yamaguchi, N.; Karino, T.; Shibayama, M.; Kornfield, J. A. *Science* **2007**, *316*, 1014–1017.

(39) Hsiao, B. S.; Yang, L.; Somani, R. H.; Avila-Orta, C. A.; Zhu, L. *Phys. Rev. Lett.* **2005**, *94*, 117802.

(40) Fijiyama, M.; Wakino, T. *J. Appl. Polym. Sci.* **1991**, *42*, 2739–2747.

(41) Fijiyama, M.; Wakino, T. *J. Appl. Polym. Sci.* **1991**, *42*, 2749–2760.

(42) Zhu, P.-W.; Edward, G. *Macromol. Mater. Eng.* **2003**, *288*, 301–311.

(43) Price, F. P. In *Nucleation*; Zettlemoyer, A. C., Ed.; Marcel Dekker: New York, 1969; pp 405−488.